This is a preprint, the final version is subject to change, of the American Mineralogist (MSA)
Cite as Authors (Year) Title. American Mineralogist, in press.
(DOI will not work until issue is live.) DOI: http://dx.doi.org/10.2138/am.2013.4236

Revised 4236

Chemistry and Radiation Effects of Davidite

Gregory R. Lumpkin*, Mark G. Blackford, and Michael Colella

Australian Nuclear Science and Technology Organisation, Locked Bag 2001, Kirrawee DC, NSW 2232, Australia

*E-mail: grl@ansto.gov.au

ABSTRACT

Davidite ($A_{1-x}M_{21}O_{38}$) samples from five different geological localities contain approximately 0.2 to 9.5 wt% UO_2 (0.02 to 0.65 atoms per formula unit) and < 0.1 to 1.3 wt% ThO_2 (< 0.01 to 0.09 atoms per formula unit). Maximum amounts of other notable cations include 3.7 wt% V_2O_3, 4.1 wt% Cr_2O_3, 2.5 wt% Y_2O_3, 5.6 wt% La_2O_3, 6.0 wt% Ce_2O_3, 4.0 wt% MnO, 2.4 wt% ZnO, 2.7 wt% SrO, and 4.9 wt% PbO. As a result of the variation in age and Th-U content, the calculated alpha decay dose ranges from ~ 0.2 to 44 × 10^{16} α/mg (~ 0.06 to 14.5 *dpa*). For samples with ages of 275-295 Ma, the critical dose for amorphization based on electron diffraction is ~ 0.8 × 10^{16} α/mg. Natural davidite is commonly altered to rutile, ilmenite, titanite, and other minor phases.

INTRODUCTION

Davidite, a member of the crichtonite mineral group, ideally $A_{1-x}M_{21}O_{38}$, is an accessory Fe-Ti-oxide mineral in plutonic, metamorphic, and hydrothermal rocks and may be an important carrier of U, Th, Y, and lanthanides. In general, crichtonite group minerals are also important host phases for transition metals (e.g., Sc, V, Cr, Mn, Zn) and other elements such as Sr, Ba, and Pb. Davidite is unusual as it exhibits a v-shaped chondrite-normalized lanthanide element distribution (Campbell and Kelly 1978). The observed chemical complexity is undoubtedly related to the range of metal cation sites available in the structure (e.g., Gatehouse et al. 1979). The observed lanthanide element pattern of davidite is due to the partitioning of light and heavy lanthanides between the large, 12-coordinated A-site and the smaller M1 octahedral site.

Gong et al. 1995 proposed the crichtonite structure type as a candidate host phase for nuclear waste disposal. Previous research on Synroc titanate ceramics (see Vance 2012 for a recent review) has shown that the crichtonite group mineral loveringite may be present as a major phase in Fe-rich formulations (Lumpkin et al. 1995). One clear advantage of this structure type is the potential to capture a range of actinides, fission products, and processing contaminants. However, there remain a number of concerns for crichtonite waste forms, including the waste loading, processing flexibility, aqueous durability, and radiation damage response. One approach to the assessment of waste form

phases is the study of natural analogues (e.g., Lumpkin 2006, Lumpkin and Geisler-Wierwille 2012) and this is the basic theme of the present investigation.

SAMPLES AND METHODS

The samples investigated in this study range in age from approximately 275 Ma to 1580 Ma (see Table 1). Davidite samples from Connecticut (D3), Norway (D2), and Australia (D6, D7) have been assigned ages of 275, 295, and 1580 Ma, respectively, based on geological data reported in previous work (e.g., Ludwig and Cooper 1984, Lumpkin and Ewing 1988, Lumpkin et al. 2012). For the sample from Mozambique (D8), we have adopted an estimated age of 600 Ma based on previous geological information and U-Th-Pb dating (Davidson and Bennett 1950, Darnley et al. 1953, Andreoli 1984). The sample from Arizona (D4) appears to have an age of approximately 145-160 Ma based on a description of the geology, mineralogy, and radiometric dating of the associated Jurassic plutonic rocks of the Quijotoa Mountains area, south-central Arizona (Pabst and Thomssen 1959, Anderson and Nourse 2005). In this paper, we use a nominal age of 150 Ma for calculation of alpha decay dose (*D*) and displacements per atom (*dpa*) for sample D4.

Additional literature data are included in Table 1 for dessauite from the Buca della Vena mine, Tuscany, Italy (Orlandi et al. (1997); loveringite from the Jimberlana intrusion, Western Australia (Campbell and Kelly 1978, Gatehouse et al. 1978); davidite-loveringite from Biggejavri, Norway (Olerud 1988); and davidite from Bidjovagge, Norway (Bjørlykke et al. 1990). The age of dessauite is not well constrained and could be related to Alpine metamorphism and compressive deformation at 27 Ma or extentional deformation at 8-12 Ma (Costagliola et al. 1999, Montomoli et al. 2005). According to published descriptions, dessauite from Italy and loveringite from Australia are partially to heavily damaged by alpha decay of Th and U, but do not appear to be completely amorphous as the grains can be restored to single crystals by heat treatment. The samples from Biggejavri and Bidjovagge have been described as amorphous and “non-metamict”, respectively.

Electron beam microanalyses, backscattered electron images, and secondary electron images were obtained from polished sections of the samples using a JEOL JSM-6400 SEM operated at 15 kV and equipped with a Noran Voyager energy dispersive spectrometer (EDX). The instrument was

operated in standardless mode; however, the sensitivity factors were calibrated for semi-quantitative analysis using a range of synthetic and natural standard materials. Analytical data were corrected for matrix effects (absorption, fluorescence, atomic number).

TEM was performed on crushed fragments dispersed on holey carbon grids using a JEOL 2000FXII TEM equipped with a Link ISIS energy dispersive X-ray (EDX) microanalysis system and operated at 200 kV. The chemistry of the davidite fragments and mineral inclusions were checked by EDX using a nominal probe size of approximately 20 nm. Spectra were acquired for 600-900 seconds live time (plus 20-30% dead time) and processed with the Link ISIS software package TEMQuant using previously established operation and calibration procedures (Lumpkin et al., 1994).

The alpha decay dose and *dpa* values were calculated from the ThO_2 and UO_2 contents according to the equations given in Lumpkin et al. (2012). The software package SRIM was used to estimate the number of displacements per alpha decay event (N_d) required for the *dpa* calculations. In this case, we set the threshold displacement energy (E_d) to 50 eV for all atoms and used a density value of 4.5 g cm^{-3}. Using these settings, we obtained N_d = 633 displacements per alpha decay, with 539 arising from the recoil nucleus (^{234}Th, 71 keV) and 94 from the alpha particle (4.2 MeV).

RESULTS

Average compositions and formulae of the davidite samples are given in Table 2 (assuming all Fe is Fe^{3+} and all U is U^{4+}). SEM-EDX analyses demonstrate that the chemical composition varies considerably from sample to sample, but individual samples are relatively uniform in composition with only limited evidence for zoning. The major chemical components of the samples investigated in this study are TiO_2 (49.4-59.9 wt%) and Fe_2O_3 (22.1-25.9 wt%). For the actinides, the U content ranges from approximately 0.2 to 9.5 wt% UO_2, but the Th content is much lower, ranging from < 0.1 to 1.3 wt% ThO_2. Maximum amounts of other elements that were consistently detected include 1.3 wt% Al_2O_3, 0.8 wt% Sc_2O_3, 3.7 wt% V_2O_3, 4.1 wt% Cr_2O_3, 2.5 wt% Y_2O_3, 5.6 wt% La_2O_3, 6.0 wt% Ce_2O_3, 0.8 wt% CaO, 4.0 wt% MnO, 2.4 wt% ZnO, 2.7 wt% SrO, and 4.9 wt% PbO. Other elements were

included in the analyses, e.g., Nb_2O_5, SiO_2, ZrO_2, Na_2O, and K_2O, but these were only detected at low levels in specific samples.

The chemical formulae were assessed on the basis of 38 oxygen atoms giving major element contents of 11.7-13.3 Ti and 5.2-6.1 Fe^{3+} atoms per formula unit (*apfu*). For the actinides we find ranges of 0.01-0.67 U and < 0.01-0.09 Th *apfu*, therefore the calculated alpha decay dose (*D*) and displacements per atom (*dpa*) will depend significantly on composition in addition to the geological age of the samples. The formula calculations also give 0.01-0.45 Al, < 0.02-0.20 Sc, < 0.02-0.91 V, < 0.01-1.02 Cr, 0.01-0.40 Y, 0.19-0.62 La, 0.02-0.65 Ce, < 0.01-1.01 Mn, < 0.02-0.50 Zn, < 0.02-0.49 Sr, and < 0.02-0.40 Pb *apfu*. The cation totals based on 38 oxygens range from ~ 21.1 to 21.6 based on the average analyses listed in Table 2 and range from 21.0 to 21.8 for all analyses obtained in this study; however, this does not take into account the potential effect of unknown amounts of Fe^{2+} on the overall stoichiometry (which would increase the cation total). Previous work by Haggerty et al. (1983) indicate cation totals of ~ 20.8 to 23.0 *apfu* for crichtonite group minerals. In comparison, the crystal structure refinement of davidite is consistent with a cation total 21.7 *apfu* based on X-ray scattering (Gatehouse et al., 1979).

A general assessment of the nature of the samples by SEM-EDX revealed evidence for alteration in samples D2, D4, D6, and D7 (Fig. 1). Sample D3 from Waterford, Connecticut, appears to be unaltered; however, backscattered electron images indicate the presence of patchy compositional zoning and cracking of the specimen (Fig. 1a). It is not known if the cracking is related to radiation damage induced volume expansion or tectonic activity. Sample D8 from the Tete Complex, Mozambique, also appears to be unaltered and has weak chemical variation across the specimen (Fig. 1b); whereas, the sample from Norway (D2) is relatively uniform in composition and exhibits minor, fine-scale alteration features along grain boundaries (Fig. 1c). Representative SEM images (Fig. 1d-f) for the samples from Arizona (D4) and South Australia (D6, D7) show that davidite is altered to a new phase assemblage consisting of either ilmenite + rutile or titanite ± rutile. Based on the above observations, the general breakdown reactions for davidite can be expressed by the following idealized reactions for the simplified Ca-U-Mn-Fe-Ti-Si-O system:

$$CaUMn_2Fe_6Ti_{12}O_{38} \rightarrow 8(Fe_{0.75}Mn_{0.25}TiO_3) + 4TiO_2 + CaO + UO_2 + 1.5O_2 \quad (1)$$

$$SiO_2 + CaUMn_2Fe_6Ti_{12}O_{38} \rightarrow CaTiSiO_5 + 11TiO_2 + UO_2 + 2MnO + 3Fe_2O_3 \quad (2)$$

$$11CaO + 12SiO_2 + CaUMn_2Fe_6Ti_{12}O_{38} \rightarrow 12CaTiSiO_5 + UO_2 + 2MnO + 3Fe_2O_3 \quad (3)$$

Equation (1) illustrates the breakdown of davidite to ilmenite + rutile, the release of Ca and U, and the potential role of oxygen in the process. Equations (2) and (3) are provided in order to show how the availability of Si and Ca may influence the relative amounts of titanite and rutile formed during the breakdown of davidite. Although not considered here, titanite may actually incorporate significant amounts of Fe, Y, and lanthanides, and minor amounts of U depending upon the local conditions.

Overall, we calculate an alpha decay dose ranges of ~ 0.2-44 $\times 10^{16}$ α/mg (~ 0.06-14.5 *dpa*) for the samples listed in Table 1. The TEM-EDX investigations demonstrate that samples D2, D4, D6, D7, and D8 have all been rendered amorphous at a dose $\geq 1 \times 10^{16}$ α/mg ($\geq$ 0.4 *dpa*). Sample D3 is the only sample that has retained crystallinity; however, the level of radiation damage varies from grain to grain due to the observed variation in ThO_2 (0.1-0.5 wt%) and UO_2 content (0.2-0.7 wt%). Electron diffraction patterns show that different parts of this sample range from highly crystalline to partially radiation damaged (Fig. 2a-c), whereas, only diffuse rings are observed for the other samples (Fig. 2d). High-resolution TEM images of thin areas of the partially damaged grains in sample D3 reveal the presence of amorphous domains within the crystalline matrix (Fig. 2e), similar to those found in other minerals such as pyrochlore, titanite, zircon, and zirconolite (Lumpkin and Ewing 1988, Hawthorne et al. 1991, Lumpkin et al. 1991, Murakami et al., 1991, Lumpkin et al. 1997).

DISCUSSION

Based on the similarity in geological age, the derived alpha decay dose and structural data obtained for samples D3 (t = 275 Ma) and D2 (t = 295 Ma) indicate that the critical dose for amorphization (D_c) for davidite within this narrow age range is ~ 0.8 $\times 10^{16}$ α/mg (~ 0.3 *dpa*). In order to track D_c versus t over a greater age range, we have constructed a dose-age plot (Fig. 3) using the data listed in Table 1. Dose ranges for the partially damaged and highly crystalline samples (open symbols) and the fully amorphous samples (black symbols) indicate that the D_c-t response is non-linear, increasing with geological age. This effect has been observed previously in natural pyrochlore,

zirconolite, and zircon (see Lumpkin and Geisler-Wierwille 2012 and references therein). Although the dose ranges obtained for samples from each locality are insufficient to bracket D_c in a comprehensive manner, some limits on the behavior of D_c with age can be established by applying the function $D_c = D_{c0} \exp(Kt)$, in which D_{c0} is the intercept dose at $t = 0$, and K is a rate constant. As shown in Figure 3, this function must be constrained to pass above the crystalline samples and below the amorphous ones, returning approximate limits of $D_{c0} = 0.34\text{-}0.68 \times 10^{16}$ α/mg and $K = 0.9\text{-}2.6 \times 10^{-9}$ yr^{-1}.

Literature data for amorphous davidite-loveringite from Biggejavri and crystallite davidite from Bidjovagge, Norway, overlap for the dose range of $5\text{-}13 \times 10^{16}$ α/mg at 1890 Ma (shaded part of symbol in Fig. 3). This is undoubtedly due to the limited X-ray diffraction work carried out on samples of variable U content. Nevertheless, the dose range noted above provides the best current estimate for the critical amorphization dose for the samples from northern Norway. A calculated median critical dose curve with $D_{c0} = 0.51 \times 10^{16}$ α/mg and $K = 1.5 \times 10^{-9}$ yr^{-1} is also shown in Figure 3 as a dashed line. Although it is satisfying that the median dose curve passes through the overlapping dose range at 1890 Ma, any further improvement in the present analysis would require additional data constrained by careful microanalysis and diffraction studies in order to bracket the critical dose of davidite over a greater range of age.

ACKNOWLEDGEMENTS

We are grateful to Sammy Leung for assistance with the SEM work. Samples used in this study were provided by Ross Pogson (Australian Museum, Sydney) and Carl Francis (Harvard University).

REFERENCES

Anderson, T.H. and Nourse, J.A. (2005) Pull-apart basins at releasing bends of the sinistral Late Jurassic Mohave-Sonora fault system. Geological Society of America Special Paper 393, p. 97-122.

Andreoli, M.A.G. (1984) Petrochemistry, tectonic evolution and metasomatic mineralisations of Mozambique Belt granulites from S. Malawi and Tete (Mozambique). Precambrian Research, 25, 161-186.

Bjørlykke, A., Cumming, G.L., and Krstic, D. (1990) New isotopic data from davidites and sulfides in the Bidjovagge gold-copper deposit, Finnmark, northern Norway. Mineralogy and Petrology, 43, 1-21.

Campbell, I.H., and Kelly, P.R. (1978) The geochemistry of loveringite, a uranium-rare-earth-bearing accessory phase from the Jimberlana Intrusion of Western Australia. Mineralogical Magazine, 42, 187-193.

Costagliola, P., Benvenuti, M., Maineri, C., Lattanzi, P., and Ruggieri, G. (1999) Fluid circulation in the Apuane Alps core complex: evidence from extension veins in the Carrara Marb63. Mineralogical Magazine, 42, 111-122.

Darnley, A.G., Horne, M.A., Smith, G.H., Chandler, T.R.D., Dance, D.F., and Preece, E.R. (1953) Ages of some uranium and thorium minerals from east and central Africa. Mineralogical Magazine, 32, 716-724.

Davidson, C.F. and Bennett, J.A.E. (1950) The uranium deposits of the Tete district, Mozambique. Mineralogical Magazine, 29, 291-303.

Gatehouse, B.M., Grey, I.E., and Kelly, P. (1979) The crystal structure of davidite. American Mineralogist, 64, 1010-1017.

Gatehouse, B.M., Grey, I.E., Campbell, I.H., and Kelly, P. (1978) The structure of loveringite – a new member of the crichtonite group. American Mineralogist, 63, 28-36.

Gong, W.L., Ewing, R.C., Wang, L.M., and Xie, H.S. (1995) Crichtonite structure type ($AM_{21}O_{38}$ and $A_2M_{19}O_{36}$) as a host phase in crystalline waste form ceramics. Materials Research Society Symposium Proceedings, 353, 807-815.

Haggerty, S.E., Smyth, J.R., Erlank, A.J., Rickard, R.S., and Danchin, R.V. (1983) Lindsleyite (Ba) and mathiasite (K): two new chromium titanates in the crichtonite series from the upper mantle. American Mineralogist, 68, 494-505.

Hawthorne F.C., Groat L.A., Raudsepp M., Ball N.A., Kimata M., Spike F.D., Gaba R., Halden N.M., Lumpkin G.R., Ewing R.C., Greegor R.B., Lytle F.W., Ercit T.S., Rossman G.R., Wicks F.J., Ramik, R.A., Sherriff B.L., Fleet M.E., and McCammon C. (1991) Alpha-decay damage in titanite. American Mineralogist, 76, 370-396.

Ludwig, K.R., Cooper, J.A. (1984) Geochronology of Precambrian granites and associated U-Ti-Th mineralization, northern Olary province, South Australia. Contributions to Mineralogy and Petrology, 86, 298-308.

Lumpkin, G.R. (2006) Ceramic waste forms for actinides. Elements, 2, 365-372.

Lumpkin, G.R. and Geisler-Wierwille, T. (2012) Minerals and Natural Analogues. In: Konings, R.J.M. (ed.), Comprehensive Nuclear Materials, volume 5, pp. 563-600, Amsterdam, Elsevier.

Lumpkin, G.R. and Ewing, R.C. (1988) Alpha decay damage in minerals of the pyrochlore group. Physics and Chemistry of Minerals, 16, 2-20.

Lumpkin G.R., Eby R.K., and Ewing R.C. (1991) Alpha-recoil damage in titanite ($CaTiSiO_5$): direct observation and annealing study using high resolution transmission electron microscopy. Journal of Materials Research, 6, 560-564.

Lumpkin, G.R., Leung, S.H.F., and Ferenczy, J. (2012) Chemistry, microstructure, and alpha decay damage of natural brannerite. Chemical Geology, 291, 55-68.

Lumpkin, G.R., Smith, K.L., and Blackford, M.G. (1995) Partitioning of uranium and rare earth elements in Synroc: effect o impurities, metal additive, and waste loading. Journal of Nuclear Materials, 224, 33-42.

Lumpkin, G.R., Smith, K.L., and Gieré, R. (1997) Application of analytical electron microscopy to the study of radiation damage in the complex oxide mineral zirconolite. Micron, 28, 57-68.

Lumpkin, G.R., Smith, K.L., Blackford, M.G., Gieré, R., and Williams, C.T. (1994) Determination of 25 elements in the complex oxide mineral zirconolite by analytical electron microscopy. Micron, 25, 581-587.

Montomoli, C., Ruggieri, G., Carosi, R., Dini, A., and Genovesi, M. (2005) Fluid source and pressure–temperature conditions of high-salinity fluids in syn-tectonic veins from the Northeastern Apuan Alps (Northern Apennines, Italy). Physics and Chemistry of the Earth, 30, 1005-1019.

Murakami T., Chakoumakos B.C., Ewing R.C., Lumpkin G.R., and Weber W.J. (1991) Alpha-decay event damage in zircon. American Mineralogist, 76, 1510-1532.

Olerud, S. (1988) Davidite-loveringite in early Proterozoic albite felsite in Finnmark, north Norway. Mineralogical Magazine, 52, 400-402.

Orlandi, P., Pasero, M., Duchi, G., and Olmi, F. (1997) Dessauite, (Sr,Pb)(Y,U)(Ti,Fe^{3+})$_{20}O_{38}$, a new mineral of the crichtonite group from Buca della Vena mine, Tuscany, Italy. American Mineralogist, 82, 807-811.

Pabst, A. and Thomssen, R.W. (1959) Davidite from the Quijotoa Mountains, Pima County, Arizona. Bulletin of the Geological Society of America, 70, 1739 (abstract).

Peterson, R.C. and Grey, I.E. (1995) Preparation and structure refinement of synthetic Ti^{3+}-containing lindsleyite, $NaMn_3Ti_{18}O_{38}$. Canadian Mineralogist, 33, 1083-1089.

Vance, E.R. (2012) Ceramic Waste Forms. In: Konings, R.J.M. (ed.), Comprehensive Nuclear Materials, volume 5, pp. 485-503, Amsterdam, Elsevier.

Table 1. Summary of the localities, age data, alpha decay dose, number of displacements per atom (dpa) of natural davidite, dessauite and loveringite.

Locality	Samples	*t* (Ma)	*D* (10^{16} α mg^{-1})	*dpa*
Tuscany, Italy[1]	—	8	0.06-0.20	0.02-0.06
	—	27	0.20-0.66	0.06-0.21
Pima County, Arizona	D4	150	1.3-2.4	0.41-0.76
Waterford, Connecticut	D3	275	0.19-0.55	0.06-0.18
Iveland, Norway	D2	295	1.0-1.4	0.35-0.44
Tete complex, Mozambique	D8	600	15-16	4.8-5.2
Radium Hill, S. Australia	D6, D7	1580	31-44	10.1-14.5
Biggejavri, Norway[2]	—	1890	3-13	1.0-3.9
Bidjovagge, Norway[3]	—	1890	5-22	1.5-6.7
Jimberlana, W. Australia[4]	—	2420	0.2-3.7	0.05-1.16

[1]Dessauite, Orlandi et al. (1997), contains 0.02-0.19 wt% ThO_2 and 2.63-8.74 wt% UO_2. [2]Davidite-loveringite, Olerud (1988), 0.84-3.51 wt% UO_2. [3]Davidite, Bjølykke et al. (1990), 0.5-2.0 wt% UO_2 [4]Loveringite, Campbell and Kelly (1978), Gatehouse et al. (1978), 0.1-0.5 wt% ThO_2 and 0.0-0.3 wt% UO_2.

Table 2. Average compositions (wt% oxides) of six davidite samples determined by SEM-EDX, including standard deviations on the mean (in parentheses) and typical 1σ minimum precision from the peak fitting procedure.

	D2	D3	D4	D6	D7	D8	1σ (%)
TiO_2	56.0	57.4	56.9	52.5	51.9	49.8	0.8
ThO_2	0.19	0.26	0.62	n.d.	0.04	n.d.	25.0
UO_2	1.42	0.36	4.46	6.96	8.86	9.14	2.5
Al_2O_3	1.16	0.34	0.51	0.62	0.28	0.64	6.6
Sc_2O_3	0.65	0.03	0.16	0.30	0.39	0.15	10.0
V_2O_3	0.15	0.27	0.44	2.70	3.36	1.83	7.5
Cr_2O_3	n.d.	0.04	0.88	0.66	1.81	3.94	8.6
Fe_2O_3	24.9	23.0	23.8	23.8	22.6	23.4	1.0
Y_2O_3	1.88	2.21	1.06	1.32	0.50	0.22	6.9
Ln_2O_3	9.9	5.0	9.5	7.9	4.1	7.2	11.8
CaO	0.23	0.16	0.65	0.32	0.11	0.40	11.1
MnO	1.24	3.64	0.10	0.15	0.43	0.12	2.4
ZnO	0.40	1.84	0.12	0.24	0.28	0.22	5.3
SrO	n.d.	0.17	0.00	0.66	2.46	1.26	8.0
PbO	0.38	3.36	0.10	1.83	2.78	0.97	4.3
Others	1.60	1.06	0.68	0.03	0.23	0.59	—
Chemical formulae based on O = 38							
Ti	12.57	13.14	12.95	12.34	12.30	11.82	
Th	0.01	0.02	0.04	0.00	0.00	0.00	
U	0.09	0.02	0.30	0.48	0.62	0.64	
Al	0.41	0.12	0.18	0.23	0.10	0.24	
Sc	0.17	0.01	0.04	0.08	0.11	0.04	
V	0.04	0.07	0.11	0.68	0.85	0.46	
Cr	0.00	0.01	0.21	0.16	0.45	0.98	
Fe	5.66	5.30	5.49	5.66	5.42	5.63	
Y	0.30	0.36	0.17	0.22	0.08	0.04	
Ln	1.06	0.55	1.04	0.88	0.46	0.83	
Ca	0.07	0.05	0.21	0.12	0.04	0.13	
Mn	0.31	0.93	0.03	0.04	0.11	0.03	
Zn	0.09	0.41	0.03	0.06	0.07	0.05	
Sr	0.00	0.03	0.00	0.12	0.45	0.23	
Pb	0.03	0.28	0.01	0.15	0.24	0.08	
Others	0.37	0.29	0.28	0.02	0.07	0.18	
Total	21.18	21.60	21.09	21.24	21.37	21.38	

Figure Captions

Figure 1. Representative SEM (backscattered electron) images. **a**) Crystalline to partially damaged davidite sample D3 from Connecticut (275 Ma) showing patchy chemical zoning. The origin of the blocky fracture pattern is unknown. Width of image = 3 mm. **b**) Weakly zoned, fully amorphous davidite sample D8 from Mozambique (~ 600 Ma). Width of image = 6 mm. **c**) Fully amorphous davidite sample D2 from Norway (295 Ma). Width of image = 5 mm. **d**) Fully amorphous davidite sample D4 from Arizona (~ 150 Ma) showing distinct alteration rim to titanite and minor rutile. Width of image = 4 mm. **e-f**). Fully amorphous davidite samples D6 (e) and D7 (f) from Australia (1520 Ma) showing various levels of alteration to ilmenite and rutile. Width of image = 8 mm (e) and 5 mm (f).

Figure 2. TEM results. **a-c**) Electron diffraction patterns of davidite sample D3 with variable alpha decay dose values of ~ 0.2, 0.3, and 0.5×10^{16} α/mg, respectively, showing the appearance of diffuse rings with increasing dose (note, this is also a function of tilt conditions and lattice orientation. **d**) Diffraction pattern of fully amorphous davidite D2 showing diffuse rings and no Bragg beams. **e**) HRTEM image corresponding to diffraction pattern in (b), showing mottled contrast due to amorphous domains in a crystalline matrix. Width of image is ~ 40 nm.

Figure 3. Plot of alpha decay dose versus geological age. Black symbols represent fully amorphous samples and open symbols represent crystalline samples. All symbols represent the observed range of dose in the vertical axis; literature data for dessauite from Italy include the possible age range from 8 to 27 Ma in the horizontal axis, resulting in the parallelogram-shaped region. Literature data for davidite from Finnmark, Norway, are shown at t = 1890 Ma, the upper black box represents amorphous davidite, the lower open box represents crystalline davidite, and the gray central box is the region where the dose values overlap. The D_c value for the Finnmark davidites should fall somewhere in this gray box. Curved lines represent the calculated critical amorphization dose constrained to pass above the crystalline samples and below the amorphous samples. Curves A and C are the approximate limits and curve B is the median value. See text for further explanation.

Figure 1

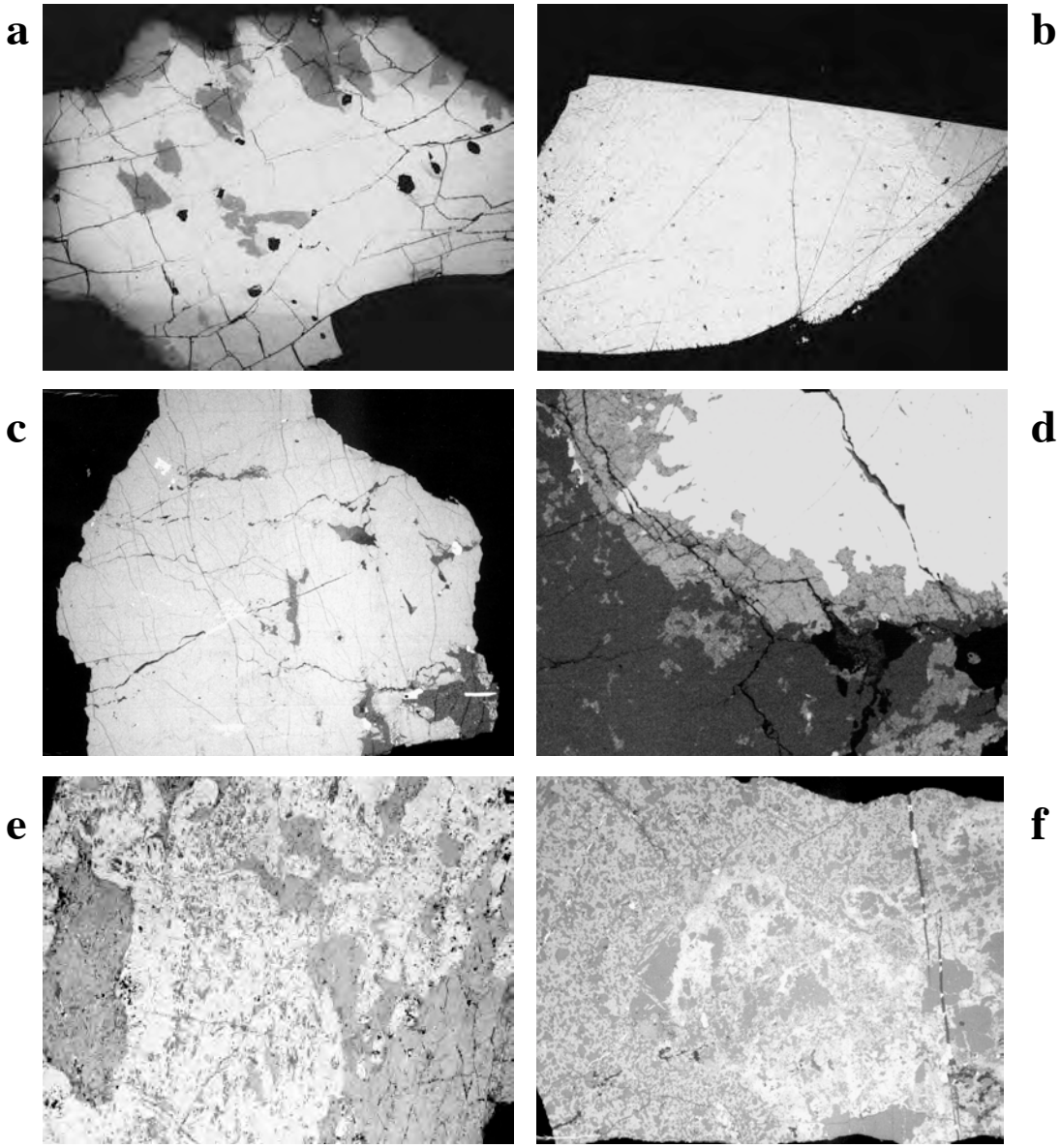

Figure 2

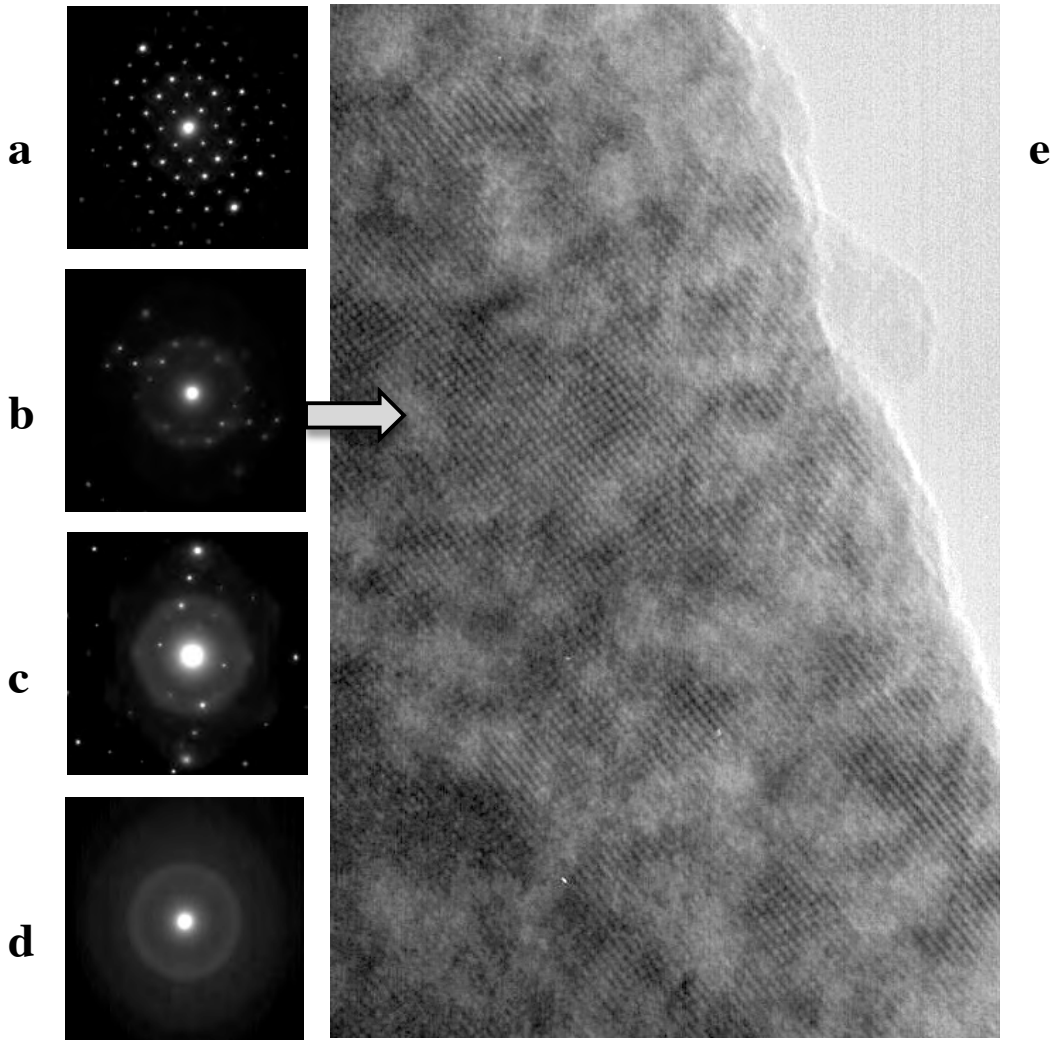

Figure 3

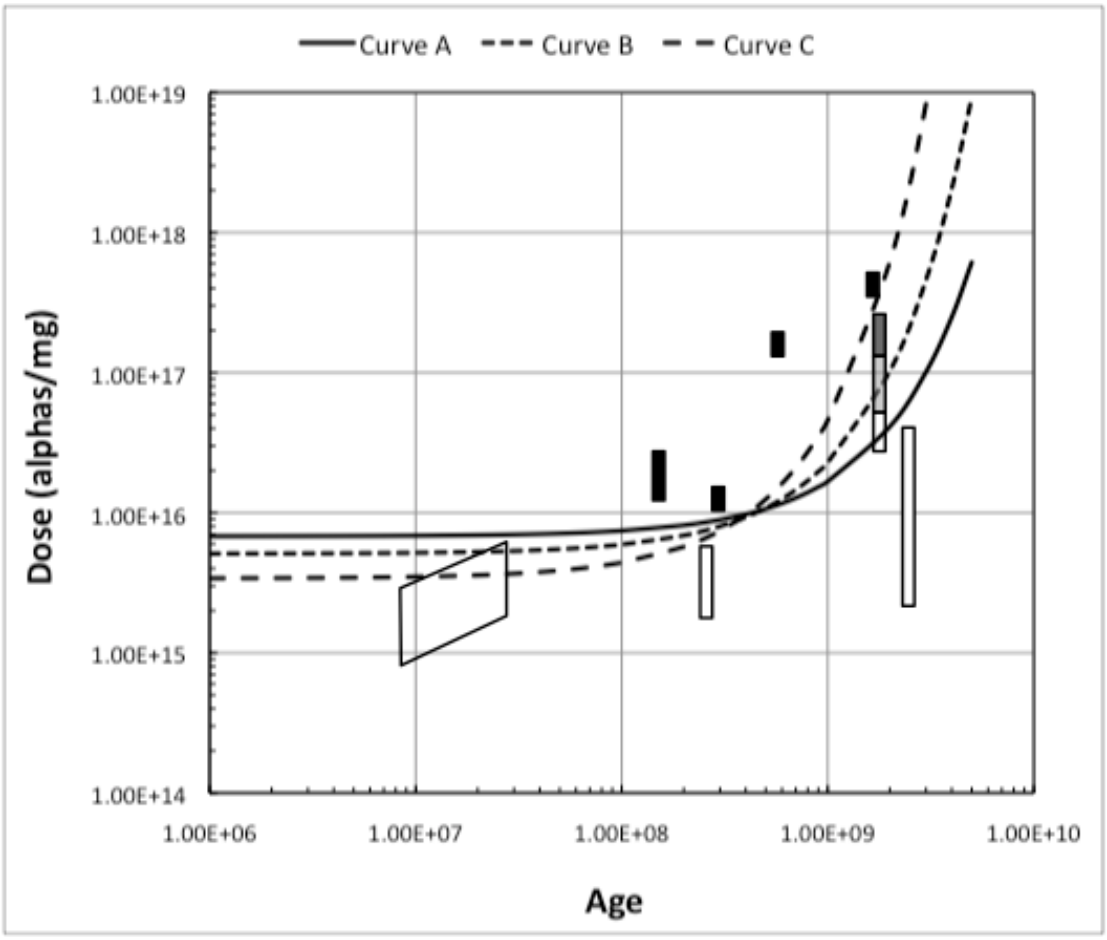
Curve A
Curve B
Curve C
1.00E+19
1.00E+18
1.00E+17
1.00E+16
1.00E+15
1.00E+14
Dose (alphas/mg)
1.00E+06
1.00E+07
1.00E+08
1.00E+09
1.00E+10
Age